57
Research paper
Doi 10.61892/STP202601027M
ISSN 2566-4484

STEPGRAD
СТЕПГРАД

Nataša Mrđa Bošnjak, University of Banja Luka, natasa.mrdja-bosnjak@aggf.unibl.org
Dragan Milašinović, University of Novi Sad, ddmilasinovic@gmail.com

INFLUENCE OF POROSITY ON ELASTO-VISCOPLASTIC BOUNDARY IN THICK-WALLED CONCRETE CYLINDER

Abstract:

In this paper, a new approach for determining the stress-strain state that incorporates spatial variations in porosity into the elasto-viscoplastic analysis of a thick-walled concrete cylinder subjected to long-term loading is presented. This approach uses rheological dynamic theory (RDT), based on the principles of mass and energy conservation. By coupling local creep-induced stress with porosity at the finite element level, the model predicts modified stress fields and changes of the elasto-viscoplastic boundary, resulting in a more accurate representation of the elastic and viscoplastic zones. The results showed that RDT provided a reliable model for estimating rheological parameters of material after exposure to long-term loads.

Keywords: RDT model, porosity, FEM, long-term load, elasto-viscoplastic boundary

УТИЦАЈ ПОРОЗНОСТИ НА ЕЛАСТИЧНО-ВИСКОПЛАСТИЧНУ ГРАНИЦУ У ДЕБЕЛОЗИДНОМ БЕТОНСКОМ ЦИЛИНДРУ

Сажетак:

У овом раду је представљен нови приступ за одређивање напонског стања који укључује просторне варијације порозности у еластично-вископластичној анализи дебелозидног бетонског цилиндра изложеног дуготрајном оптерећењу. Овај приступ користи реолошку динамичку теорију (РДТ), засновану на принципима очувања масе и енергије. Усљед везе локалног напона изазваног течењем са порозношћу на нивоу коначних елемената, модел предвиђа модификована поља напона и промене еластично-вископластичне границе, што резултира тачнијим приказом еластичних и вископластичних зона. Резултати су показали да РДТ пружа поуздан модел за процену реолошких параметара материјала након излагања дуготрајним оптерећењима.

Кључне ријечи: РДТ модел, порозност, МКЕ, дуготрајно оптерећење, еластично-вископластична граница

1. INTRODUCTION

Concrete structures in civil engineering commonly develop cracks as a result of void initiation, growth, and eventual coalescence. Such voids typically originate around inclusions due to particle fracture or loss of adhesion at the particle–matrix interface. Environmental influences—including mechanical loading, elevated temperatures, freeze–thaw cycles, and exposure to aggressive media modify the pore size distribution, spatial arrangement, and overall porosity of hardened concrete. These effects are directly associated with the void volume fraction (VVF). Rheological dynamics provides relationships between the VVF and mechanical characteristics by measuring, with non-destructive methods only P and S wave velocities, because it is based on the propagation of elastic waves. Since these parameters are associated with long-term loading, rheological dynamics, grounded entirely in theoretical principles, provides an appropriate framework for obtaining results concerning long-term loads.

Recent studies on the elastoplastic behavior of concrete structures subjected to long-term loading have primarily focused on the development and propagation of plastic zones using advanced constitutive models that combine plasticity, damage, and creep effects [1], [2]. Numerous works employ continuum-based elastoplastic formulations, such as Drucker–Prager or concrete damage plasticity models, to capture the evolution of stress and strain fields in axisymmetric or thick-walled structural elements, including cylinders and pressure vessels [3]. In these approaches, the boundary between elastic and plastic regions is typically determined based on stress-based creep criteria and time-dependent material parameters. Although some studies account for microstructural degradation or creep-induced softening under sustained loading [4], [5], porosity is generally treated as a homogenized material property, without an coupling between local porosity variations and the corresponding local stress state governing the elastoplastic transition.

In contrast, the present work introduces a localized and explicit consideration of porosity in the elasto-viscoplastic analysis of a thick-walled concrete cylinder subjected to long-term loading. Rather than assuming porosity as a global or averaged material parameter, the proposed formulation establishes a direct relationship between porosity and local stresses, allowing spatial variations in porosity to influence the mechanical response at the material-point level. This coupling leads to modified stress distributions and, consequently, to new predictions of the displacement of the elasto-viscoplastic boundary within the cylinder wall. As a result, the extent of the elastic and viscoplastic zones evolves differently compared to conventional models reported in the literature, where such interactions are neglected. By integrating porosity and stress in a localized manner, this study provides a novel framework for analyzing elasto-viscoplastic zone evolution in porous concrete structures, thereby extending existing elasto-viscoplastic theories toward a more physically representative description of concrete microstructure effects.

2. MODEL DESCRIPTION ACCORDING TO RDT

The rheological-dynamic modulus is the real part of the complex modulus of elasticity derived from the rheological-dynamical analogy (RDA), where stress is generally considered a time-varying function. This quantity represents a very important link between several parameters, and for quasi-static problems the expression for the RDA modulus E_R is presented in the following form, which connects the modulus of elasticity E_H and the creep coefficient φ in the viscoplastic (VP) region.

$$E_R = E_H \frac{1}{1+\varphi} \tag{1}$$

Milašinović in [6] applies the equation that Bernoulli established for an incompressible fluid to solid matter by observing the passage of the strain energy density through two cross sections. Based on this, he derives the relationship between the creep coefficient φ and Poisson's ratio μ in the following form:

$$\varphi = \frac{2\mu}{1-2\mu} \tag{2}$$

In wave propagation, the creep coefficient reduces to the ratio of two moduli:

$$\varphi = \frac{E_H}{H'} \tag{3}$$

where H' is the VP modulus.
As reported in [7], [8], the creep coefficient is assumed to vary linearly with porosity and is expressed as follows:

$$\varphi(p) = \varphi_1 - \frac{p(\varphi_1 - \varphi_E)}{p_E} \tag{4}$$

where φ_1 is at zero porosity, while φ_E is at the end of the porosity interval [0, p_E]. p_E is defined at the end of measurable porosity. On the other hand, due to points (p_E, φ_E) and $(p_{max}, 0)$, the creep coefficient φ_E is:

$$\varphi_E = \varphi_1 \left(1 - \frac{p_E}{p_{max}}\right) \tag{5}$$

The creep coefficient varies linearly with the elastic modulus, whereas the VP modulus is independent of porosity due to the principle of mass conservation. As a result, Eq. (2) establishes a linear relationship between the elastic modulus and porosity.
According to the RDA, the relationship between the Poisson's ratio and porosity for the interval [0, p_E] is

$$\mu_{RDA}(p) = \left[\varphi_1 - \frac{p(\varphi_1 - \varphi_E)}{p_E}\right] \Big/ \left\{2\left[1 + \varphi_1 - \frac{p(\varphi_1 - \varphi_E)}{p_E}\right]\right\} \tag{6}$$

Consequently, the nonlinear relationship between the damage variable and porosity is:

$$D(p) = \left[\varphi_1 - \frac{p(\varphi_1 - \varphi_E)}{p_E}\right] \Big/ \left\{1 + \left[\varphi_1 - \frac{p(\varphi_1 - \varphi_E)}{p_E}\right]\right\}. \tag{7}$$

3. RELATIONSHIP BETWEEN RDT PARAMETERS AND DAMAGE MECHANICS

If ψ denotes the quotient of the elastic modulus and the dynamic modulus for which expressions can be obtained via the P and S wave velocities, then Poisson's ratio via the wave velocities can be written in the following form, according to [9]:

$$\mu_{1/2} = \frac{(\psi - 1) \pm \sqrt{\psi^2 - 10\psi + 9}}{4} \tag{8}$$

By substituting the expression for the RDA modulus, which is derived for quasi-static problems, into the formula for deformation derived according to RDA, and then including this result in the equation for the critical creep coefficient, a quadratic equation is obtained in [10]. The solution to this equation can be presented in the following form, based on two Poisson's ratios:

$$\sigma_i = \frac{1}{2K_{E,i}}\left(\sqrt{1 + 4K_{E,i}E_i(0)\varepsilon} - 1\right), \quad i = 1,\ 2, \tag{9}$$

Where K_E is defined as the material constant at the elastic limit, while $E(0)$ is the elastic modulus of the material in the undamaged state:

$$K_{E,i} = \frac{\varphi_i}{\sigma_{ef}}, \quad \varphi_i = \frac{2\mu_i}{1-2\mu_i}, \quad E_i(0) = E_H(1+\varphi_i), \qquad i = 1,\ 2, \tag{10}$$

The effective stress σ_{ef} can be understood to represent not only the effect of reducing the geometric cross-section area due to damage, but also includes the effects of stress concentration in voids or the effects of interaction between voids, [11]

$$\sigma_{ef} = \frac{f_{cS}}{1-D_1}, \tag{11}$$

where f_{cS} is the uniaxial unconfined compressive strength (UCS) of the damaged dry sample.

In [8], Milašinović gave a detailed explanation of the limit values of VVF based on the strain energy densities shown in Figure 1, where

$$W_{el} = \frac{1}{2E_H}\sigma_{ef}^2,$$

$$\begin{aligned} W_{d1} &= \int_0^{\varepsilon_{cF}} \sigma_1 d\varepsilon = \int_0^{\varepsilon_{cF}} \frac{1}{2K_{E1}}\left(\sqrt{1+4K_{E1}E_1(0)\varepsilon}-1\right)d\varepsilon = \\ &= \frac{1}{2K_{E1}}\left[-\varepsilon_{cF} + \frac{-1+\left(1+4K_{E1}E_1(0)\varepsilon_{cF}\right)^{3/2}}{6K_{E1}E_1(0)}\right], \end{aligned} \tag{12}$$

$$\begin{aligned} W_{d2} &= \int_0^{\varepsilon_{cF}} \sigma_2 d\varepsilon = \int_0^{\varepsilon_{cF}} \frac{1}{2K_{E2}}\left(\sqrt{1+4K_{E2}E_2(0)\varepsilon}-1\right)d\varepsilon = \\ &= \frac{1}{2K_{E2}}\left[-\varepsilon_{cF} + \frac{-1+\left(1+4K_{E2}E_2(0)\varepsilon_{cF}\right)^{3/2}}{6K_{E2}E_2(0)}\right]. \end{aligned}$$

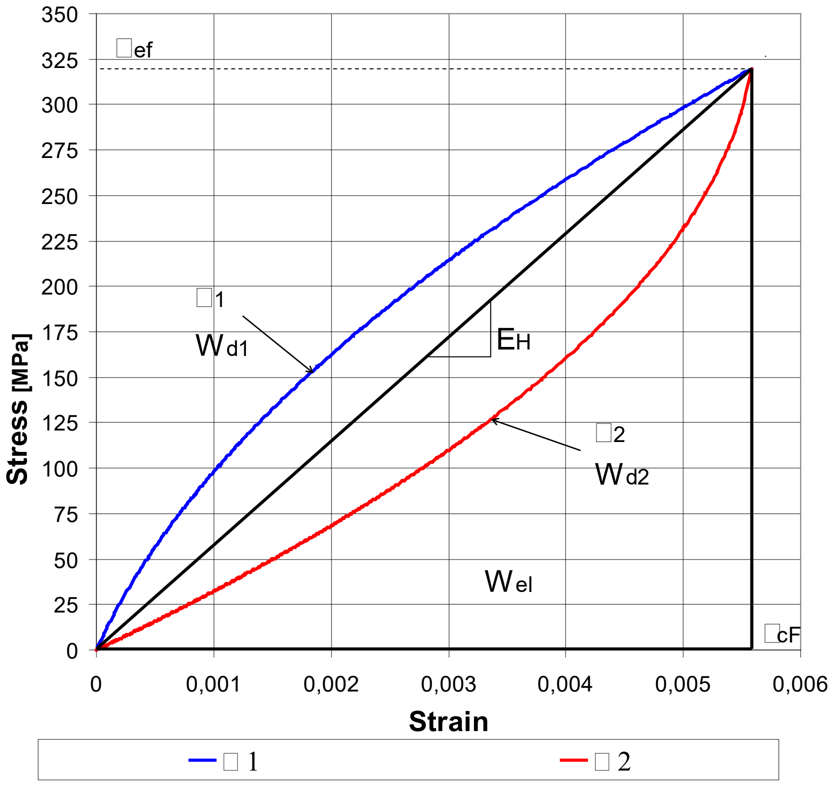

Figure 1. Strain energy densities: with positive Poisson's ratio (blue line) and with negative (red line) (created by author).

The total energy density dissipation is

$$W_d = W_{d1} - W_{d2} \tag{13}$$

Consequently, the maximum VVF can be determined as follows

$$p_{max} = \frac{W_d}{W_{el}} = \frac{W_{d1} - W_{d2}}{W_{el}}. \tag{14}$$

It is well known that a positive Poisson's ratio is a measurable value, and a negative one is not. This fact allows us to determine the limit of measurable VVF

$$p_E = \frac{W_{d1} - W_{el}}{W_{el}}. \tag{15}$$

Using the difference between the W_{d1} and W_{d2} in relation to the W_d, the VVF which controls the macroscopic failure of the sample by the static strength f_{US2} [10] is

$$p_f = \frac{2W_{el} - W_{d1} - W_{d2}}{W_d}. \tag{16}$$

The previous difference in relation to the W_{el}, defines the minimum VVF which controls the dynamic strength f_{US1}

$$p_{min} = \frac{2W_{el} - W_{d1} - W_{d2}}{W_{el}}. \tag{17}$$

4. DETERMINATION OF POROSITY BY FINITE ELEMENTS ACCORDING TO RDT

In [12] the relationship between the strength and the stress at the limit of elasticity is determined

$$\frac{\sigma_E}{f_{cS}} = \frac{\varphi_1}{1+\varphi_1} = D_1 . \tag{18}$$

Numerous studies indicate that the progression of damage or strength degradation in concrete does not follow a linear pattern [13], [14] . Thus, the nonlinear correlation between porosity and the strength of dry VP material σ_f, according to the RDT as is derived in [8], is

$$\sigma_f = \sigma_{ef} \left\{ 1 - \frac{p_f}{p_E} \left[1 - D_1 \left(1 - D_f \right) \right] \right\} \tag{19}$$

where p_E is the porosity at the end of the measurable porosity range, while D_f is a porosity-dependent damage variable.
The solution to the previous equation is found by reducing it to a quadratic equation, expressed in the following form:

$$p = \frac{-b - \sqrt{b^2 - 4ac}}{2a} \tag{20}$$

where the coefficients *a*, *b* and *c*, are

$$a = \varphi_1 \tag{21}$$

$$b = \varphi_1 p_E \left(\frac{\sigma_f}{\sigma_{ef}} - 1 \right) - p_{\max} \left(1 + \varphi_1 - D_1 \right) \tag{22}$$

$$c = p_{\max} \left(1 + \varphi_1 \right) p_E \left(1 - \frac{\sigma_f}{\sigma_{ef}} \right) . \tag{23}$$

Porosity by element is obtained when we apply equations (20), (21), (22) and (23) to each element. The given equations take the following form, [8], [15], [16]:

$$p_{fe} = \frac{-b - \sqrt{b^2 - 4ac}}{2a} \tag{24}$$

$$a = \varphi_1 \tag{25}$$

$$b = \varphi_1 p_E \left(\frac{\sigma_{fe}}{\sigma_{ef}} - 1 \right) - p_{\max} \left(1 + \varphi_1 - D_1 \right) \tag{26}$$

$$c = p_{\max} \left(1 + \varphi_1 \right) p_E \left(1 - \frac{\sigma_{fe}}{\sigma_{ef}} \right) \tag{27}$$

where the stress σ_{fe} was obtained according to FEM analysis in time *t*, taking creep into account.
This approach enables the evaluation of time-dependent material properties for all porous finite elements within the discretized finite element mesh. Using the computed porosity values, the elastic modulus can be determined assuming a linear relationship between porosity and Young's modulus:

$$E_{H,fe}(p) = E_{H0,fe}\left(1 - \frac{p_{fe}}{p_{\max,fe}}\right). \tag{28}$$

The values of the creep coefficient and Poisson's ratio by elements are calculated according to the following expressions, respectively [8]:

$$\varphi_{fe}(p) = \varphi_1\left(1 - \frac{p_{fe}}{p_{\max,fe}}\right) \tag{29}$$

$$\mu_{fe}(p) = \frac{\varphi_{fe}(p)}{2\left(1+\varphi_{fe}(p)\right)}. \tag{30}$$

5. DRUCKER-PRAGER YIELD CRITERION

The behavior of materials is governed by the Drucker-Prager yield criterion, which is commonly used to analyze materials such as rocks and concrete, [17]. The Drucker–Prager yield criterion differs from the von Mises criterion, which is based exclusively on the deviatoric component of the stress tensor. In contrast, the Drucker–Prager criterion incorporates the hydrostatic component of the stress state. It was formulated as a modification of the Mohr–Coulomb creep criterion. The model can be expressed mathematically as follows:

$$f(I_1, J_2) = BI_1 + \sqrt{J_2} - A = 0 \tag{31}$$

that is, expressed through the principal stresses:

$$\sqrt{\frac{1}{6}\left[(\sigma_1-\sigma_2)^2 + (\sigma_2-\sigma_3)^2 + (\sigma_3-\sigma_1)^2\right]} = A + B(\sigma_1+\sigma_2+\sigma_3). \tag{32}$$

In (31), parameters A and B represent positive material constants that can be determined from the yield stress during uniaxial compression and tension tests, σ_c and σ_t, [8-9], where I_1 is the first invariant of the Cauchy stress tensor and J_2 is the second invariant of the deviatoric part of the Cauchy stress tensor.

- Relation between Mohr-Coulomb parameters and Drucker-Prager parameters

The angle of internal friction for the DP criterion (β) is obtained through expression (33) from the angle of internal friction for the MC criterion (φ):

$$\tan\beta = \frac{3\sqrt{3}\tan\varphi}{\sqrt{9+12\tan^2\varphi}}. \tag{33}$$

Cohesion for DP criterion (d) is obtained through expression (34) from the angle of internal friction for MC criterion (φ) and cohesion for MC criterion (c):

$$d = \frac{3\sqrt{3}c}{\sqrt{9+12\tan^2\varphi}}. \tag{34}$$

Cohesion is not entered directly into the DP criterion, but through the yield stress, which for the DP condition is calculated via cohesion from expression (35):

$$\sigma_c{}^0 = \frac{d}{1-\frac{1}{3}\tan\beta}. \tag{35}$$

6. ANALYSIS OF A THICK-WALLED CONCRETE CYLINDER

A section of concrete thick-walled concrete cylinder 1 m long is observed, analyzed with the appropriate conditions of symmetry, with r_1=100(mm) inner radius and r_2=200(mm) outer radius.

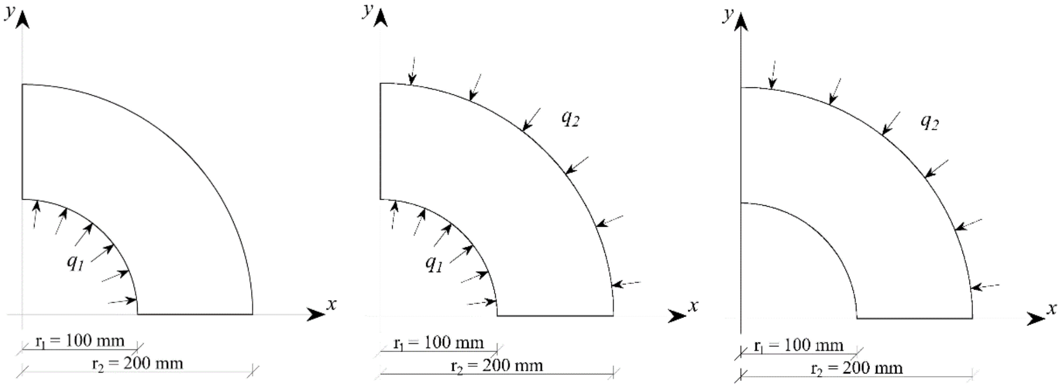

Figure 2. Quarter cross-section of a thick-walled cylinder with internal pressure (left), internal and external pressure (middle), and external pressure (right) (created by author).

It will be assumed that the cylinder is long enough so that the effects from the ends are not felt on the part being observed. SG concrete tested experimentally in [18] was used for the material used to model the cylinder. Concrete SG was obtained on samples cast in standard cylindrical molds with a diameter of 150 mm and a height of 300 mm, and an age of 28 days. The selected concrete can be classified as non-standard, given that it has high strength, but also high deformability compared to other types of concrete. Concrete SG is commercially known as SikaGrout®-212 (powdered concrete mixture consisting of: cement, crushed stone aggregate and powdered cement additives)[19]. Experimental data for SG concrete is given in Table 1:

Table 1. Parameters of SG concrete obtained experimentally

μ	E_H (MPa)	f_c (MPa)	f_t (MPa)	f_b (MPa)	ρ (kg/m3)
0.185	30994.00	65.88	9.00	65.90	2265.5

The parameters needed to calculate the parameters taking into account the porosity, calculated according to the RDA, are given in Table 2:

Table 2. Calculated parameters according to RDA for SG concrete, required for the calculation of porosity by elements

E_H (MPa)	φ_1	P_E	σ_{ef}	p_{max}	D_1	$E_{H,0}$ (MPa)
30994.00	1.67	0.2085	175.93	0.5119	0.6255	38046.8

6.1. CYLINDER LOADED ON THE INNER EDGE WITH AND WITHOUT VVF

In the first example (Figure 2 – left), the cylinder is loaded with an internal pressure of intensity *q=18.44(N/mm)*. The results are given in cylindrical coordinates (*r, θ, z*), and for the part of the load that gives a response within the limits of elasticity, it is compared with the known analytical solution [20]:

$$\sigma_r = q\frac{r_1^2}{r_2^2 - r_1^2}\left(1 - \frac{r_2^2}{r^2}\right) \tag{36}$$

$$\sigma_\theta = q\frac{r_1^2}{r_2^2 - r_1^2}\left(1 + \frac{r_2^2}{r^2}\right) \tag{37}$$

where r is the observed radius on the cylinder that defines the position for which the answer is obtained, σ_r is radial stress, and σ_θ is hoop stress.

The cross-section of the cylinder is modeled as a plate with the Drucker-Prager (DP) model in Abaqus, i.e. a model in which the inelastic part of the response is obtained by adopting the Drucker-Prager yield condition. By analyzing the convergence of the results, it was found that for a mesh with an element size of 1 mm, the solution converged, and the given element size was used for further analyses. For the DP model - a quadrilateral, four-node, bilinear, plane strain element, without reduced integration (CPE4) was used from the Abaqus library,[21], [22].

The required input characteristics calculated according to RDT [23] for associative flow were calculated for the Mohr–Coulomb (MC) creep condition (Table 3) after which the relationships between the parameters of the Mohr-Coulomb creep condition and the Drucker-Prager creep condition were used to obtain the parameters required for the model in Abaqus according to the expressions (33), (34) and (35). The values of the obtained required input characteristics are given in the Table 4.

Table 3. SG concrete parameters required for MC material modeling

μ	E_H (MPa)	φ (°)	ψ(°)	*c*(MPa)	f_t (MPa)
0.31277	30994.00	44.331	44.331	25.78	21.71

In Table 3, φ denotes the angle of internal friction, ψ denotes the angle of dilatancy, and c denotes cohesion.

Table 4. SG concrete parameters required for DP material modeling

μ	E_H (MPa)	β (°)	ψ(°)	K	σ_c^0 (MPa)
0.31277	30994.00	48.3015	48.3015	1	47.329

In Table 4, β denotes the angle of internal friction for DP material, K is the coefficient that defines the shape of the yield surface in the deviator plane. For the classic Drucker-Prager hypothesis, it is assumed that K=1, whereby the yield surface in the deviatoric stress plane is circular.

6.1.1. Cylinder analysis considering only the effect of creep without porosity

A comparison of the elastic solution obtained analytically according to the expressions (35) and (36) with the solution obtained on the numerical model for the MC model and the DP model was performed. The results confirmed the validity of the model (Figure 3) and the solution beyond the elastic limits was analyzed on the given model, for the last load increment in the Figure 4.

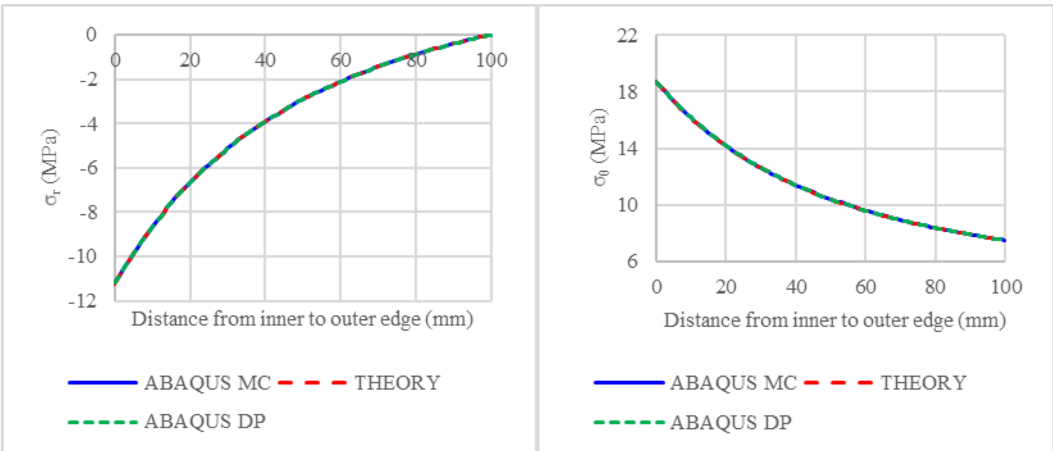

Figure 3. Radial stress (left) and hoop stress (right) obtained theoretically and with Abaqus for MC and DP model (created by author).

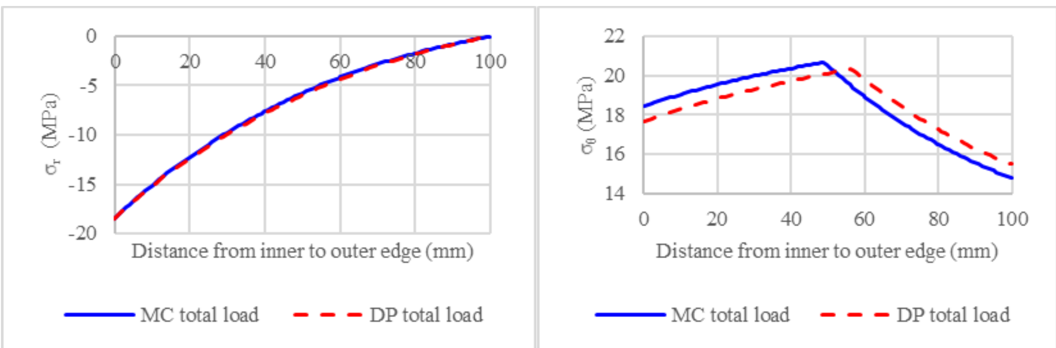

Figure 4. Radial stress (left) and hoop stress (right) obtained for MC and DP model for the last load increment - total load (created by author).

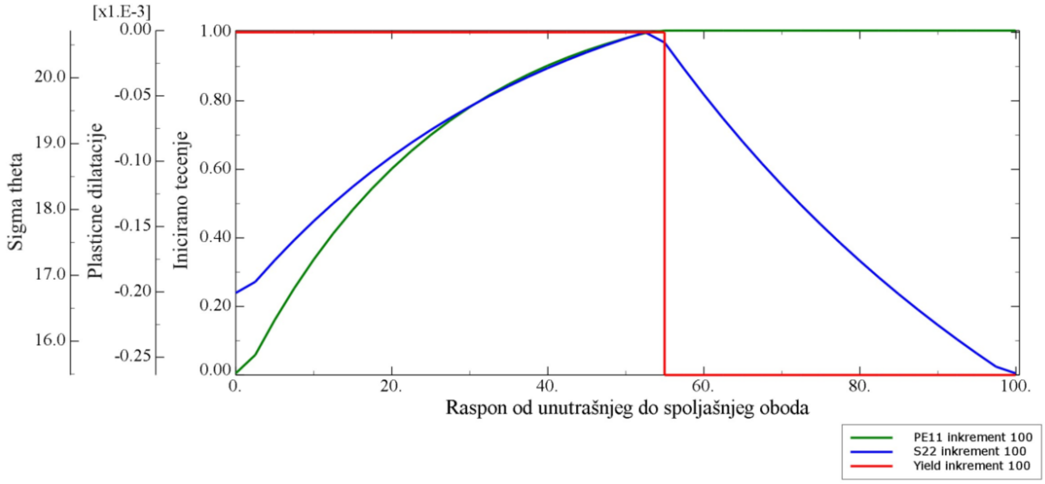

Figure 5. Viscoplastic dilatations, hoop stress and limit of viscoplastic and elastic region for total load (created by author).

It can be concluded that after a radius of 157.464 mm there is no VP deformation.

6.1.2. Cylinder analysis considering the effect of creep and porosity

Based on the radial stresses obtained from Abaqus per element in the last increment, and the material data obtained according to RDA given in Table 2, the porosities per element, elastic modulus and Poisson's ratio for each element are calculated. After that, in the same model, new elastic moduli and Poisson's ratios are assigned to the elements, and the calculation is repeated to obtain displacement values with the influence of porosity.

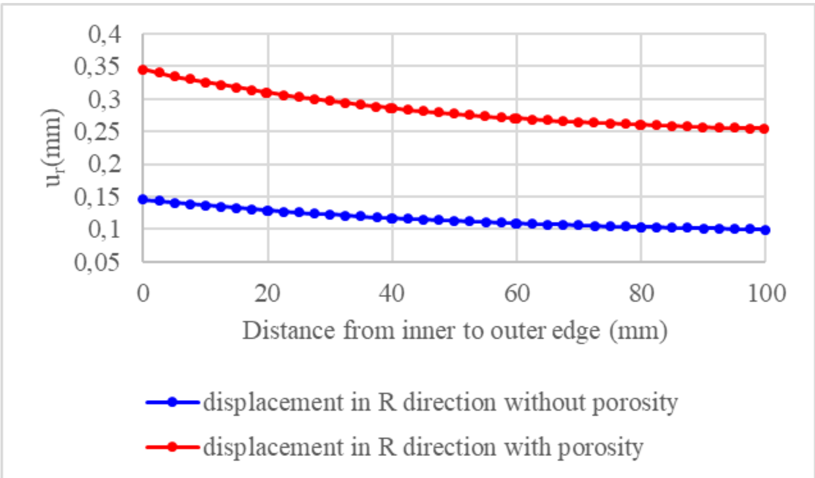

Figure 6. Comparison of displacement in the radial direction without and with the influence of porosity according to RDA (created by author).

According to the previously described model for calculating porosity by elements, displacements in the direction of the radius without and with the influence of porosity according to RDA are obtained and compared, (Figure 6.)

It can be concluded that the displacements obtained are more than twice as large when porosity is taken into account compared to the displacements obtained only due to the influence of creep.

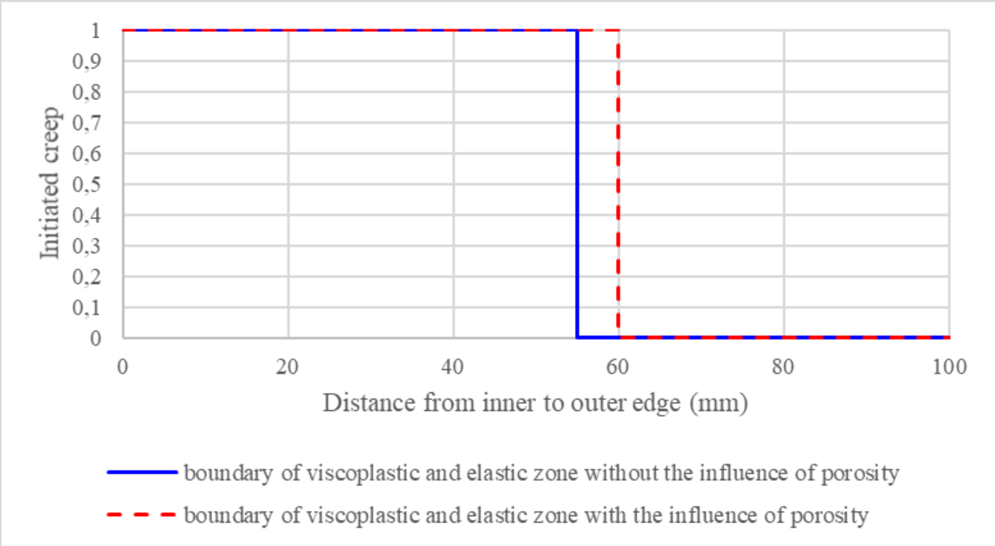

Figure 7. The limits of the viscoplastic and elastic region for the total load with and without the effect of porosity (created by author).

When we take into account the porosity according to RDA in the calculation, after a radius of 159.925 mm there is no VP deformation.

From the Figure 7 it can be seen that the boundary of the VP and elastic region has changed by taking porosity into account, i.e. without the influence of porosity it is $r_{el\text{-}vpl}$=157,464(mm), i.e. a smaller value is obtained compared to the value obtained by taking porosity into account, which is $r_{el\text{-}vpl}(p)$=159.925(mm).

6.2. CYLINDER LOADED ON THE INNER AND OUTER EDGE WITH AND WITHOUT VVF

In this example, the cylinder is loaded with an internal pressure of intensity q_1=18.44(N/mm) and an external pressure of intensity q_2=65.88(N/mm), (Figure 2 - middle), and for the part of the load that gives a response within the elastic limits, it is compared with the known analytical solution and elastic limits:

$$\sigma_r = \frac{\sigma_{Rcc} r_1^2 - \sigma_3 r_2^2}{r_2^2 - r_1^2} + \frac{(\sigma_3 - \sigma_{Rcc}) r_1^2 r_2^2}{\left(r_2^2 - r_1^2\right) r^2} \tag{38}$$

$$\sigma_\theta = \frac{\sigma_{Rcc} r_1^2 - \sigma_3 r_2^2}{r_2^2 - r_1^2} - \frac{(\sigma_3 - \sigma_{Rcc}) r_1^2 r_2^2}{\left(r_2^2 - r_1^2\right) r^2} . \tag{39}$$

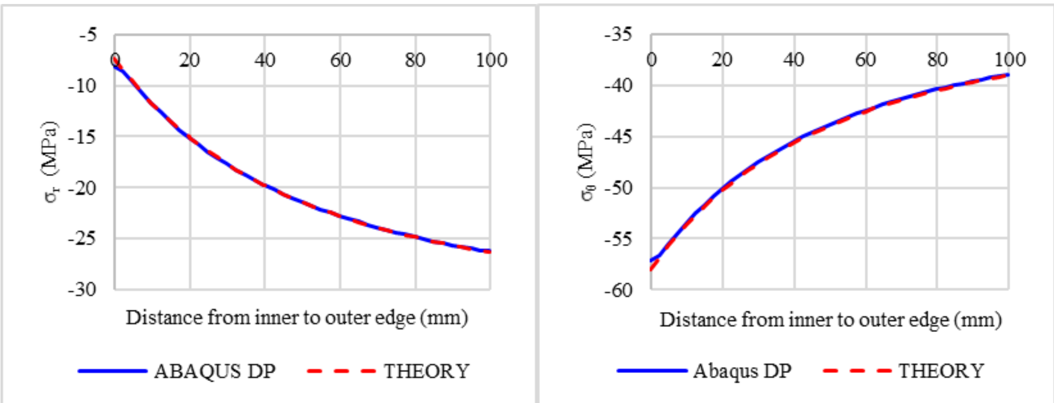

Figure 8. Radial stress (left) and hoop stress (right) obtained theoretically and with Abaqus for DP model – comparison for elastic solution (created by author).

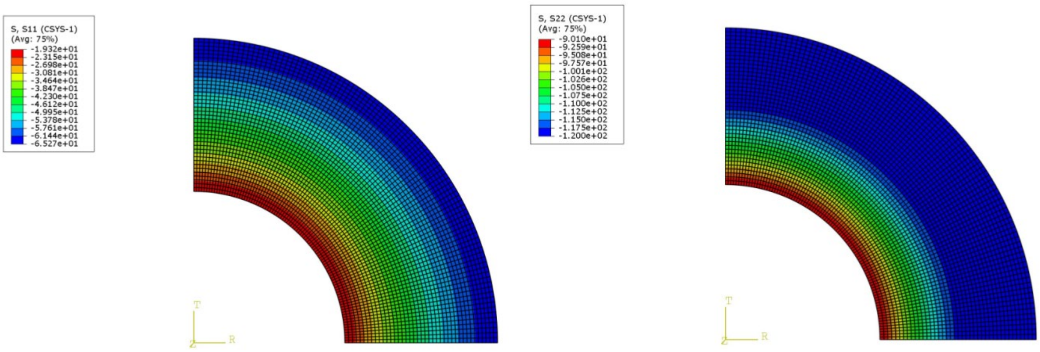

Figure 9. Radial stress (left) and hoop stress (right) obtained with Abaqus for DP model for the last load increment - total load (created by author).

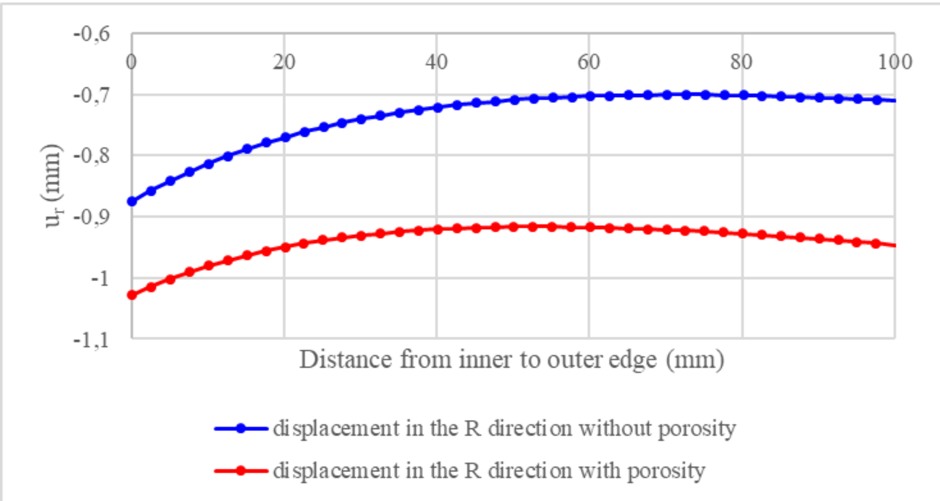

Figure 10. Comparison of displacement in the radial direction without and with the influence of porosity according to RDT (created by author).

Figure 8 shows the solutions from the last increment that does not give VP deformation. The VP deformation occurs after the 40th increment. Based on the radial stresses obtained from Abaqus per element in the last increment (Figure 9), and the material data obtained according to RDA given in Table 2, the porosities per element, elastic modulus and Poisson's ratio for each element are calculated, according to the procedure described in the first example and new displacement values in the radial direction are obtained. In Figure 10, a comparison of displacement in the radial direction without and with the influence of porosity according to RDA is shown.

6.3. CYLINDER LOADED ON THE OUTER EDGE WITH AND WITHOUT VVF

The example analyzed is a cylinder loaded only with external pressure of intensity q_2=50(N/mm) (Figure 2 – right). An example without the influence of porosity is analyzed and the obtained radial stress values (Figure 11) are used to obtain the VVF values according to the presented RDA procedure:

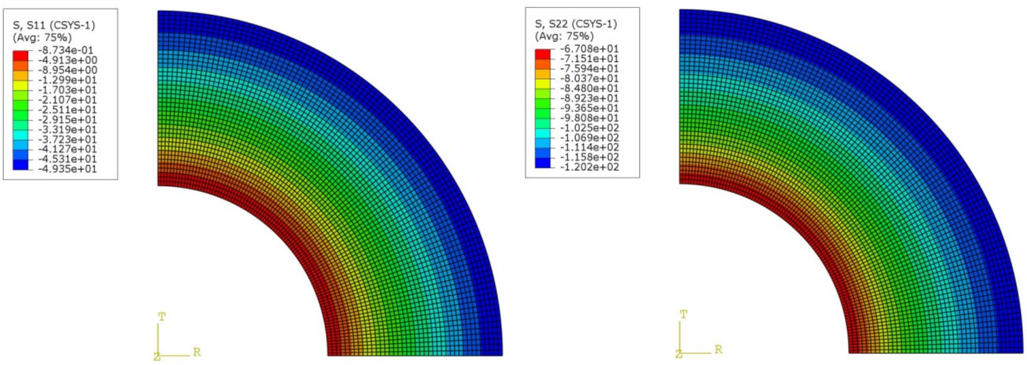

Figure 11. Radial stress (left) and hoop stress (right) obtained with Abaqus for DP model for the last load increment - total load (created by author).

Figure 12 shows the displacement values without and with the influence of porosity according to the RDA.

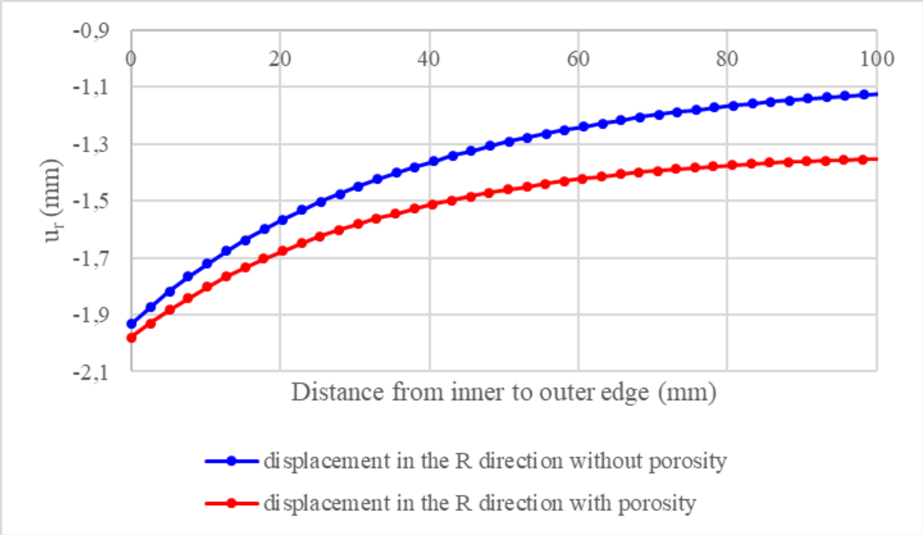

Figure 12. Comparison of displacement in the radial direction without and with the influence of porosity according to RDA (created by author).

7. CONCLUSIONS

In this paper, a new method presented in [8] for obtaining porosity from energy densities in the context of rheological dynamics is analyzed. The essence of the proposed method for introducing porosity effects is that porosity, in terms of aggregate pores and cracks (VVF), is related to structural loading because stresses in the structure change under load. With the aim of showing as precisely as possible the impact of damage in structures on the stress-strain state of porous materials, a new numerical method was developed that defines the modulus of elasticity locally, by finite elements, and depends on the stress state caused by the influence of creep obtained by applying RDT [16].

By applying the Drucker-Prager creep criterion, the model was introduced into the VP domain of analysis through the example of a thick-walled concrete cylinder.

For the part of the load that provides solutions in the elastic domain, a comparison with the analytical solution was made and the model was validated through the given examples. The example of a thick-walled concrete cylinder subjected to internal pressure shows that taking into account porosity leads to the appearance of a larger elastic zone compared to the example without the influence of porosity, which was established by determining the radius that is the boundary of the elastic and VP zone without the influence of porosity and with the influence of porosity. The displacements with the influence of porosity in this example, in the radial direction, are more than twice as large as the displacements obtained without the influence of porosity. The example of thick-walled concrete cylinder subjected to internal and external pressure corresponds to a special case in which tunnels can be found at very great depths (tunnels at depths of approximately 1000m) and for this example displacements were also analyzed, and the results showed that displacements due to the influence of porosity are also greater than displacements when porosity is not taken into account. The example of a thick-walled concrete cylinder subjected to external pressure corresponds to the classic case of a tunnel whose zone around the inner radius was degraded during excavation, and this case of loading also showed that the displacements in the radial direction with the influence of porosity are slightly higher compared to the displacements obtained when porosity is not taken into account.

By analyzing the impact of porosity on the stress-strain state of the structure after long-term exposure to loading, with reference to the behavior of the material in the elastic and border zone of the transition to the VP zone, results were obtained that clearly indicate that porosity significantly affects the distribution of stress, and has a direct impact on the expansion of the elastic area.

LITERATURE

[1] A. Dummer, M. Neuner, and G. Hofstetter, “An extended gradient-enhanced damage-plasticity model for concrete considering nonlinear creep and failure due to creep,” *Int. J. Solids Struct.*, vol. 243, May 2022, Art. no. 111541, doi: 10.1016/J.IJSOLSTR.2022.111541.

[2] X. Ren, Q. Wang, R. Ballarini, and X. Gao, “Coupled Creep-Damage-Plasticity Model for Concrete under Long-Term Loading,” *J. Eng. Mech.*, vol. 146, no. 5, Feb. 2020, Art. no. 04020027, doi: 10.1061/(ASCE)EM.1943-7889.0001748.

[3] W.-F. Chen, *Plasticity in reinforced concrete*. New York: McGraw-Hill, 1982.

[4] Z. P. Bažant and M. Jirásek, “Creep and hygrothermal effects in concrete structures,” *Solid Mech. its Appl.*, vol. 225, pp. 1–921, 2018, doi: 10.1007/978-94-024-1138-6/COVER.

[5] Y. Zhang, T. Sun, M. Qin, D. Zhang, N. Qin, and Y. Wang, “Effect of Time and Stress on Creep Damage Characteristics of Cement-Based Materials,” *Build. 2024, Vol. 14, Page 3745*, vol. 14, no. 12, Nov. 2024, Art. no. 3745, doi: 10.3390/BUILDINGS14123745.

[6] D. D. Milašinović, “Rheological-dynamical analogy: Modeling of fatigue behavior,” *Int. J. Solids Struct.*, vol. 40, no. 1, pp. 181–217, 2003, doi: 10.1016/S0020-7683(02)00518-8.

[7] D. Milašinović, D. Goleš, A. Rožnjik, and N. M. Bošnjak, “Model of porous materials by rheological-dynamical analogy using the principles of mass and energy conservation,” *Int. Conf. Contemp. Theory Pract. Constr. / Међународна конференција Савремена теорија и пракса у градитељству*, no. 15, pp. 092–103, Jun. 2022, doi: 10.7251/STP2215092M.

[8] D. D. Milašinović, “Modeling of porous-hardened concrete by rheological-dynamical analogy,” *Eng. Comput. (Swansea, Wales)*, vol. 40, no. 9/10, pp. 2615–2647, Dec. 2023, doi: 10.1108/EC-08-2022-0574/FULL/XML.

[9] D. D. Milašinović, D. Majstorović, and R. Vukomanović, “Quasi static and dynamic inelastic buckling and failure of folded-plate structures by a full-energy finite strip method,” *Adv. Eng. Softw.*, vol. 117, pp. 136–152, Mar. 2018, doi: 10.1016/j.advengsoft.2017.07.013.

[10] D. D. Milašinović, “Rheological-dynamical method for prediction of compressive strength and deformation of rocks,” *Int. J. Rock Mech. Min. Sci.*, vol. 141, May 2021, Art. no. 104659, doi: 10.1016/j.ijrmms.2021.104659.

[11] S. Murakami, *Continuum Damage Mechanics*, vol. 185. Dordrecht: Springer Netherlands, 2012.

[12] D. D. Milašinović, “Rheological–dynamical analogy: visco-elasto-plastic behavior of metallic bars,” *Int. J. Solids Struct.*, vol. 41, no. 16–17, pp. 4599–4634, Aug. 2004, doi: 10.1016/j.ijsolstr.2004.02.061.

[13] X. Chen, D. Shi, and S. Guo, “Experimental Study on Damage Evaluation, Pore Structure and Impact Tensile Behavior of 10-Year-Old Concrete Cores After Exposure to High Temperatures,” *Int. J. Concr. Struct. Mater.*, vol. 14, no. 1, pp. 1–17, Mar. 2020, doi: 10.1186/s40069-020-0393-5.

[14] L. Xu, Y. Duan, and Y. Li, “Porosity, gradient and impact velocity effects on compressive response of foamed concrete,” *Constr. Build. Mater.*, vol. 315, Jan. 2022, Art. no. 125616, doi: 10.1016/J.CONBUILDMAT.2021.125616.

[15] D. D. Milašinović *et al.*, “Porosity Effects on Folded-Plate Structures by Finite Strip Method and Rheological Dynamics,” *Int. J. Civ. Eng.*, 2024, doi: 10.1007/s40999-024-01065-x.

[16] N. Mrđa Bošnjak, D. D. Milašinović, D. Goleš, J. Gučević, and A. Ceh, “Porosity Effects on the Composite Girder by Rheological Dynamics and FEM,” *Materials (Basel).*, vol. 17, no. 23, 2024, Art. no. 5779, doi: https://doi.org/10.3390/ma17235779.

[17] D. C. Drucker and W. Prager, “Soil mechanics and plastic analysis or limit design,” *Q. Appl. Math.*, vol. 10, no. 2, 1952, doi: 10.1090/qam/48291.

[18] D. D. Milašinović, “Rheological-dynamical continuum damage model for concrete under uniaxial compression and its experimental verification,” *Theor. Appl. Mech.*, vol. 42, no. 2, pp. 73–110, 2015, doi: 10.2298/tam1502073m.

[19] D. D. Milašinović, S. Bursać, N. Mrđa Bošnjak, and A. Čeh, “Critical void volume fraction of concrete,” *J. Fac. Civ. Eng.*, vol. 40, pp. 17–17, 2024, doi: 10.14415/CACE2024.07.

[20] W. F. Chen and D. J. Han, *Plasticity for Structural Engineers*. 1988.
[21] Dassault, “ABAQUS User’s Manual,” *ABAQUS/CAE User’s Man.*, pp. 1–847, 2012.
[22] Dassault Systèmes Simulia Corp., *Abaqus Theory Manual*. 2011.
[23] D. D. Milašinović, “Rock failure mechanisms based on rheological dynamics,” *J. Rock Mech. Geotech. Eng.*, 2024, doi: doi.org/10.1016/j.jrmge.2024.04.036.